Intermediate isobar effects in a two-nucleon mechanism for (p,π)

M. J. Iqbal*
Physics Department, Indiana University, Bloomington, Indiana 47405
and Physics Department, University of Maryland, College Park, Maryland 20742

G. E. Walker
Physics Department, Indiana University, Bloomington, Indiana 47405
(Received 27 August 1984; revised manuscript received 25 April 1985)

Results are presented for a two-nucleon model of the (p,π) reaction in the resonance region. Features of the microscopic two-nucleon model adopted include propagating intermediate pions and rho mesons, and an intermediate delta isobar whose propagator includes interaction with the nuclear system as well as an energy dependent width. Realistic distorted waves are adopted for the external proton and pion. Transitions from a closed shell to two-particle—one-hole and single-particle final states are studied, with both projectile- and target-emission diagrams included, for a carbon target. The results indicate that the effect of finite range delta propagation is important in lowering the sensitivity of the predictions to the details of proton and pion distortions and the bound state wave functions. The results are not very sensitive to the exact nature of the delta-nucleus interaction. The relative magnitude of target-emission or projectile-emission diagrams depends on the particular transition and angle under consideration. Comparison with experiment and future extensions and applications of the model are discussed.

I. INTRODUCTION

There now exists precise experimental data on the (p,π) reaction at intermediate energies ($150 \leq T_p \leq 800$ MeV) for a wide variety of nuclear targets and final states. Unfortunately theoretical progress has not kept pace and there does not yet exist a satisfactory theory of proton-induced pion production on complex nuclear targets.[1] The existing data is often characterized as being largely devoid of systematic trends. The process is characterized by a large momentum transfer, Q, to the nucleus ($Q > 2k_f$). Thus, approaches that involve only a single nucleon in the production process [single nucleon mechanism (SNM)] are known to be very sensitive to the details of pion and proton optical potentials and the form of the bound single nucleon orbitals.[1] In the plane wave limit the SNM cross section is proportional to $|\phi(Q)|^2$, where ϕ is the final bound state nucleon orbital. Since Q is very large the details of the orbital at large Q are emphasized. Moreover, since one effect of optical potential-induced distortions is to "smear out" the values of Q at which ϕ is evaluated, the details of optical potentials which allow lower "effective" Q values become crucial.

There exists considerable motivation for suggesting that a two-nucleon mechanism (TNM) is more important and appropriate for describing the (p,π) reaction. In the TNM the transition operator incorporates explicitly the interaction of the projectile nucleon with one of the target nucleons. For intermediate energy protons, an important piece of the TNM should involve virtual isobar (Δ) production with subsequent isobar propagation and decay to the final bound nucleon and emitted pion (see Fig. 1). It is known that pion rescattering with intermediate isobar formation is extremely important for pion production in the two-nucleon system in the range $200 \leq T_p \leq 400$ MeV.[1] This fact has been known for almost 30 years.[2] More recent successful theories of pion production in the two-nucleon system have also adopted a model with an intermediate Δ with *static* transition potentials.[3] Whether such models are sufficient for explaining spin observables in the two-body system is still under investigation. The additional approximations required for embedding such a two-body theory in the many-body environment (i.e., validity of a *distorted waves* theory) are not yet stringently tested. Before such finer tests are possible it seems necessary, as a first step, to treat the intermediate isobar formation more carefully than previously has been done in the many body problem. In a complex nucleus the TNM allows the large momentum transfer to be shared among two active nucleons (or, equivalently, among three bound nucleon orbitals). Also the (p,π⁻) process, which requires two nucleons to change their charge (in a nucleons-only model), can be naturally incorporated in a TNM, as can transitions to two-particle—one-hole (2p-1h) final states from an initial closed shell nucleus. Transitions to final states characterized as 2p-1h have been found to be prominent in (p,π) excitation spectra.[4]

Earlier investigations utilizing a TNM have been suggestive of the validity of the approach but cannot yet be considered definitive or capable of quantitative predictions because of the approximations employed.[5–9] Previous investigations have either utilized the zero-range approximation for the intermediate meson and/or have not allowed for explicit propagation of the isobar in the nucleus. The propagation of the intermediate particles effectively introduces nonlocalities in the nuclear transition matrix elements. Because such nonlocalities can themselves change the sensitivity of the final results to input

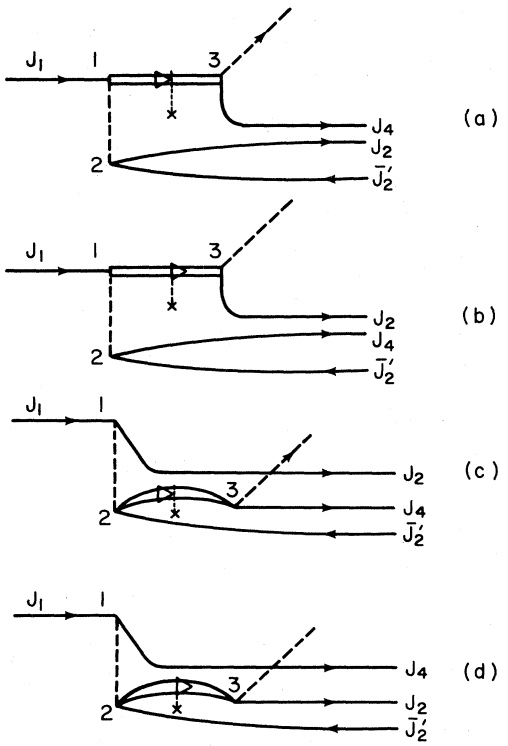

FIG. 1. Diagrammatic representation of the pion production two-nucleon mechanism assuming formation of an intermediate Δ. A two-particle—one-hole (2p-1h) final nuclear state has been assumed. The incident nucleon line is labeled by j_1, the interacting intermediate Δ is represented by a dashed line ending at a cross, the intermediate meson (ρ or π) propagating between vertices 1 and 2 is denoted by a dashed line. The final observed pion is emitted from vertex 3 and is represented by a dashed line. The final 2p-1h nuclear state is represented by the solid lines labeled j_2, j_4, and $\bar{j}'_2$. Parts (a) and (b) [(c) and (d)] are referred to as target (projectile) emission diagrams. The different labelings of the final nucleon particle states arise naturally from antisymmetrization of the nuclear wave function.

distortion and bound state wave functions, it seems important to carry out TNM calculations where the zero-range and closure approximations are not adopted.

In what follows we present results obtained using a TNM of pion production. The intermediate mesons (i.e., pion or rho) and delta propagate with the only approximation being that the interaction of the delta with the many-nucleon environment, appearing in the delta propagator, is assumed to be a local function of the nuclear density.

The results given in this paper are the first part of a systematic treatment of the TNM mechanism incorporating an intermediate propagating and interacting delta, with virtual pion and rho exchange, including the effects of realistic external proton and pion distortions. In this first discussion we work in the resonance region where contributions from the nonresonant background are expected to be small. In fact we have already extended the model to include, microscopically, nonresonant S and P wave terms. A later contribution, reporting results of (p,π) calculations near the production threshold, will contain the details of the nonresonant background extension of the present model.

In the next section we discuss the basic assumptions and input required in the model. We also include representative formulae which were used in the calculations. The details of the derivations of these equations are either briefly summarized or discussed in the appendices.

In Sec. III we present the numerical results of applying the TNM model to study pion production from a carbon ground state in the initial proton energy region $200 \leq T_p^{\text{lab}} \leq 300$ MeV. Both "single particle" and "two-particle—one-hole" final nuclear states were studied. The sensitivity of the results to distorted wave and bound state wave function parameters, intermediate delta propagation and interaction, and inclusion of both intermediate π and ρ mesons is studied in some detail. We also consider the relative importance of projectile emission and target emission diagrams (see later discussion).

Finally, in Sec. IV we discuss the results obtained in Sec. III. Implications of the results for future comparison between theory and experiment are summarized. Further theoretical and experimental research in pion production is also suggested in this section.

II. THE TWO-NUCLEON PION PRODUCTION MODEL

In this section we discuss the model adopted, and representative expressions obtained, for studying pion production from complex nuclei. For definiteness, we shall consider in this section a closed shell ($N=Z$) nuclear target ground state ($J=T=0$) and 2p-1h final nuclear states. Analogous expressions for single particle nuclear final states are given in Ref. 10.

In this initial investigation we include post-pion emission diagrams only [see Fig. 2(a)]. Pre-pion emission diagrams [see Fig. 2(b)] are expected to be generally smaller

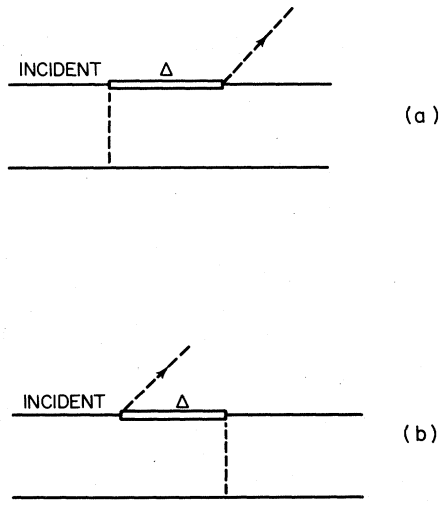

FIG. 2. (a) Post-pion emission diagram. (b) Pre-pion emission diagram. Diagrams of type (a) are included in the results discussed in the present investigation.

than the post-pion emission diagrams. By taking ratios of the energy propagators appearing in the two types of diagrams we estimate that near the resonance region ($T_p \sim 300$ MeV) the *amplitude* of the pre-emission terms should be approximately 20% of the included post-emission amplitudes. In this work we concentrate on diagrams including an intermediate $\Delta(3-3)$ resonance contribution.

The diagrams associated with contributions to the TNM interaction Hamiltonian including an intermediate Δ are shown in Figs. 1(a)—(d). We shall concentrate, as an example, on the contribution due to Fig. 1(c). One can write this contribution to the amplitude as

$$A^{(c)} = \sum_I \langle f \mid V(\mathbf{r}_3) \frac{\mid I \rangle \langle I \mid}{E_f - E_I} V(\mathbf{r}_1, \mathbf{r}_2) \mid i \rangle \ , \tag{1}$$

where $\mid i \rangle$, $\mid I \rangle$, and $\mid f \rangle$ refer to the initial, intermediate, and final states of the system, respectively. In Eq. (1), $V(\mathbf{r}_1, \mathbf{r}_2)$ represents the two-body transition operator that connects an initial two-nucleon state with an intermediate nucleon-delta state. $V(\mathbf{r}_3)$ is the one-body transition potential at the N$\Delta\pi$ vertex. Note that Figs. 1(a) and (b) [1(c) and (d)] are referred to as target (projectile) emission diagrams. In what follows we have suppressed the isospin contribution to various matrix elements and diagrams. The isospin factors are discussed separately later in this section for the various diagrams of interest.

The expression for the required matrix elements of $V(\mathbf{r}_1, \mathbf{r}_2)$, as well as the procedures for constructing the initial and intermediate states, are discussed in Appendix A. The matrix elements of $V(\mathbf{r}_3)$ and the construction of the final state are discussed in Appendix B. Combining Eqs. (A16), (A28), and (B13) we obtain the following schematic result for the nonisospin part of the matrix element appropriate for Fig. 1(c):

$$\begin{aligned} A = G_{i=\pi,\rho} \frac{f_i}{M_i} \left[\frac{f_i^*}{M_i} \right]^2 & \int_0^\infty q^2 C_{\lambda i}(q) D_i(q) G_i(\Lambda, q)\, dq [E_\Delta - M_\Delta + i\Gamma_\Delta(E_\Delta)/2 - \Sigma_\Delta]^{-1} \\ & \times \int_0^\infty dr_1 R_{n_2 l_2 j_2}(r_1) j_{\lambda_1}(q r_1) U_{lj}(k_p, r_1) \\ & \times \int_0^\infty dr_2 r_2 R_{n_\Delta l_\Delta j_\Delta}(r_2) j_{\lambda_2}(q r_2) R_{n_2' l_2' j_2'}(r_2) \\ & \times \int_0^\infty dr_3 r_3 R_{n_\Delta l_\Delta j_\Delta}(r_3) R_{n_4 l_4 j_4}(r_3) F[\phi_{l_\pi}(k_\pi, r_3)] \ , \end{aligned} \tag{2}$$

where G represents a sum over geometric, statistical, and normalization factors defined and discussed in the appendices. The sum over $i = \pi, \rho$ arises from allowing both an intermediate pion (π) and rho (ρ) meson.

The symbols $R_{n_i l_i j_i}$ represent bound nucleon wave functions [see Fig. 1(c)], $R_{n_\Delta l_\Delta j_\Delta}$ is an intermediate Δ wave function, and the $U_{l_1 j_1}(k_p, r_1)$ come from a partial wave expansion of the initial proton distorted wave. The Bessel functions, $j_\lambda(qr)$, arise from using the Fourier transform of the transition potential $V(r_1, r_2)$. The term $F[\phi_{l_\pi}(k_\pi), r_3)]$ includes derivative operators acting on the final pion partial wave decomposed distorted wave function, ϕ_{l_π} (see Appendix B). The $C_{\lambda i}(q)$ are factors arising from a multipole expansion of the intermediate pion or rho transition potential, the $D_i(q)$ are the intermediate meson propagators, and the $G_i(\Lambda, q)$ are the (monopole) form factors associated with the baryon-baryon-meson vertices.

The propagator associated with the intermediate delta is discussed in detail in Appendix C. We note that the propagator contains an energy dependent width $\Gamma_\Delta(E)$ and a contribution from a Δ-nucleus interaction Σ_Δ. The treatment of the delta propagator follows closely that outlined in Ref. 12 and is discussed here in Appendix C.

The isospin factors are straightforward to calculate. The detailed procedure is contained in Ref. 10 and is available from the authors on request. We briefly summarize the order of coupling and the results below. We assume an isospin zero target. In the nuclear intermediate state the delta isospin and nucleon particle state isospin are first coupled and the resultant isospin (t_3) and nucleon-hole-state isospin are combined to give total isospin $T_0 M_0$, i.e., we have

$$\sum_{t_3} [(\tfrac{3}{2} \otimes \tfrac{1}{2})^{t_3} \otimes \tfrac{1}{2}_{\text{hole}}]^{T_0 M_0} \ . \tag{3}$$

For the 2p-1h final state the coupling scheme is

$$\sum_{t_4} [[\tfrac{1}{2}(4) \otimes \tfrac{1}{2}(2)]^{t_4} \otimes \tfrac{1}{2}_{\text{hole}}(2')]^{T_f M_f} \ , \tag{4}$$

where (4), (2), and (2') refer to the states labeled j_4, j_2, and j_2' in Fig. 1(c), respectively. Using the order of coupling defined above and the isospin operators given in Appendices A and B for the one- and two-body transition operators, we find the isospin factor for Fig. 1(c) is

$$\tfrac{4}{3} \left[1 + \frac{1}{\sqrt{3}} \right] \quad \text{for } T_f = \tfrac{1}{2} \tag{5a}$$

and

$$\tfrac{1}{3}\sqrt{2/3} \quad \text{for } T_f = \tfrac{3}{2} \ . \tag{5b}$$

For Fig. 1(b) the isospin factors are the same as those given in Eqs. (5a) and (5b). For Figs. 1(a) and (d) the $T_f = \frac{3}{2}$ isospin factors are the same as those given in Eq.

(5b), while, for the $T_f=\frac{1}{2}$ factors, the expression in parentheses in Eq. (5a) becomes $(-1+1/\sqrt{3})$.

Of course, in addition to the 2p-1h diagrams shown in Fig. 1 there are transitions leading to single particle final states (see Fig. 3). The derivation and final formulae for transitions associated with these diagrams are similar to the results given in Appendices A and B and discussed above.

The numerical techniques for carrying out the indicated integrations including the intermediate particle propagators are nontrivial but technical in detail. The procedures adopted are discussed elsewhere.[10] One interesting feature is the difference in the pion propagator for the projectile and target emission pieces. The pion propagator may be written

$$D(q)=-\frac{1}{q^2-q_0^2+m^2-i\epsilon}\ , \tag{6}$$

where in writing Eq. (6) we have ignored the interaction of the exchanged pion with the background many-nucleon system. We are working with a nonrelativistic theory so that one might argue that the q_0^2 term should also be ignored in Eq. (6). One could also argue that, for the target emission piece (where the Δ is formed from the incident nucleon), q_0 is just the difference in the binding energies of the particle-hole pair at the NN vertex. Thus, for the final states we consider, q_0 is a few MeV, $m^2-q_0^2>0$, and the pion propagator cannot develop a pole for real q.

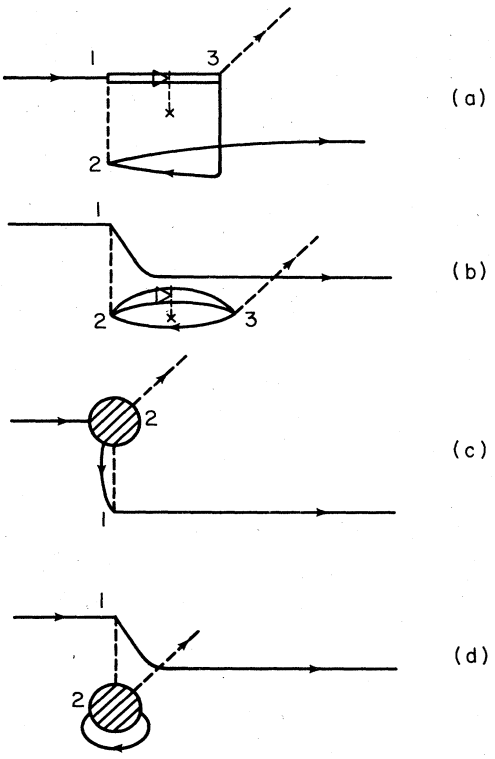

FIG. 3. Similar to Fig. 1 except a single valence particle final state has been assumed and the nucleon labels have been deleted. Diagrams (a) and (b) are Δ resonance contributions while diagrams (c) and (d) represent nonresonant contributions.

In this case the integration over q yields no imaginary part.

For the projectile emission piece, on the other hand, q_0 is the sum of the kinetic energy of the incident proton and the binding energy of the final proton bound state. For a 250 MeV proton, $q_0>250$ MeV. Thus the pion propagator can develop a pole at $q_0^2=(q^2+m^2)$, corresponding to the propagation of an on-shell pion. In this case the integral over q has complex values. Notice that in this discussion, although we have not used a static approximation for the pion propagator, integration over q_0 is eliminated because the *energy* of the intermediate pion is assumed known, since the final states have definite binding energies. In the following we summarize the distorted wave input used to generate the numerical results presented in Sec. III.

A. Proton distortions

The radial part of the proton distorted wave $U_{lj}(k,r)$ satisfies the following Schrödinger equation:

$$\left[-\frac{\hbar^2}{(2\mu)}\frac{d^2}{dr^2}+\frac{\hbar^2 l(l+1)}{2\mu r^2}+V(l,j,r)-E\right]U_{lj}(k,r)=0\ , \tag{7}$$

where μ is the reduced mass of the proton-nucleus system in the proton-nucleus center of mass and E is the corresponding energy related to the wave number k in the proton-nucleus c.m. system by

$$k^2=(E^2-\mu^2c^4)/\hbar^2c^2\ . \tag{8}$$

The quantity $V(l,j,r)$ is the proton-nucleus optical potential and is given by

$$V(l,j,r)=V_{\rm Coul}+V_1f_1+iW_2f_2 -\frac{2}{r}\left[V_3\frac{df_3}{dr}+iV_4\frac{df_4}{dr}\right](\mathbf{l}\cdot\boldsymbol{\sigma})\ . \tag{9}$$

Here $V_{\rm Coul}$ is the Coulomb potential arising from a uniform charge distribution, V_1 and W_2 represent the strengths of the real and the imaginary parts of the central potential, and V_3 and W_4 are the corresponding strengths for the spin-orbit part of the optical potential. The f's are the form factors and taken to be of the Woods-Saxon form,

$$f_i(r)=\frac{1}{1+\exp[(r-R_i)/a_i]}\ , \tag{10}$$

where a_i is the skin thickness and R_i is the radius of the potential well. The parameters adopted for the proton-nucleus optical potentials are given in Table I. The values given in Table I should be used only with relativistic kinematics. The parameters given in Table I are taken from Ref. 13 and have been obtained from fits to proton-nucleus elastic scattering in the energy range $200\le T_{\rm p}\le 350$ MeV.

TABLE I. Proton-nucleus optical potential parameters for incident proton kinetic energies of 250 and 200 MeV. Potential strengths are in MeV and R_i's and a_i's are in fm (Ref. 13).

250 MeV				200 MeV			
V_1	W_2	V_3	W_4	V_1	W_2	V_3	W_4
−6.0	−32.0	−3.1	3.5	−7.27	−28.46	−3.26	3.08
R_1	R_2	R_3	R_4	R_1	R_2	R_3	R_4
1.37	0.800	0.850	0.850	1.374	0.816	0.880	0.880
a_1	a_2	a_3	a_4	a_1	a_2	a_3	a_4
0.500	0.800	0.550	0.550	0.483	0.854	0.553	0.526

B. Pion distortions

For the calculations shown in this work we have used a modified Kisslinger potential with the center of mass correction. The modified Kisslinger potential (for a nucleus of atomic number A) is of the following form:

$$V_{\rm opt}(r)=-Ab_0k^2\rho(r)+Ab_1\nabla\cdot\rho(r)\nabla - A/2[(T_\pi+m)/M]b_1\nabla^2\rho(r)\ . \quad (11)$$

Here M is the nucleon mass, k is the wave number of the pion in the pion-nucleus c.m., T_π is the pion kinetic energy, and b_0 and b_1 are parameters related to the S- and P-wave pion-nucleon phase shifts. For 250 and 200 MeV proton kinetic energies and a ^{12}C target we use the following values for the complex parameters b_0 and b_1:[14]

T_p=250 MeV	
Reb_0=−0.43	Imb_0=0.56
Reb_1=7.11	Imb_1=3.32

T_p=200 MeV	
Reb_0=−0.44	Imb_0=0.29
Reb_1=9.00	Imb_1=1.14

The radial part of the pion distorted wave, ϕ_l, has been generated using the program PIRK.[15]

Finally, the relation between the individual amplitudes associated with the diagrams shown in Figs. 1 and 3 and the cross section is given in the c.m. system by[16]

$$\frac{d\sigma}{d\Omega}=\frac{1}{(2\pi)^2}\left[\frac{k_\pi}{k_p}\right](E_\pi E_p)\frac{E^A E^{A+1}}{(E^{\rm tot})^2}\frac{1}{2}\left|\sum Amp\right|^2, \quad (12)$$

where E_π, E_p, E^A, and E^{A+1} refer to the energies of the final pion, incident proton, initial target, and final target, respectively.

III. RESULTS

The TNM discussed in Sec. II has been applied to obtain the numerical results reported in this section. Since the most important new feature associated with the present model is the incorporation of an intermediate, propagating delta, we focus first on the *sensitivity* of the results to the parameters appearing in the delta propagator. Results for subsections A and B below include only the pion contribution to the one-boson exchange transition potential leading to NN→ΔN.

A. Sensitivity of results to the (free) width and delta-nucleus potential appearing in the delta propagator

We consider first the effect of the delta-nucleus potential on the predicted angular distribution for ^{12}C(p,π^+)^{13}C$_{\rm g.s.}$ at $T_p^{\rm lab}$=250 MeV. For these illustrative calculations we have assumed a simple closed shell for the ^{12}C ground state and a single valence $1p_{1/2}$ neutron for the ^{13}C ground state. Harmonic oscillator single particle orbitals with oscillator parameter $\beta=m\omega/h=0.3718$ fm^{-2} were adopted. For the incident proton energy under consideration the Δ-nucleus potential parameters (see Sec. II) are $V=-19.37$ MeV, $W=-42.7$ MeV. If the free width for the Δ is used we have $\Gamma=110$ MeV. If we use the standard result for the energy dependent width $\Gamma(E)$, then

$$\Gamma(E)=\frac{f^2}{6\pi m_\pi^2}\frac{k^3(k^2+M_N^2)^{1/2}}{\sqrt{S}}\ , \quad (13)$$

where $\sqrt{S}$ is the total energy in the pion-nucleon c.m. (πN c.m.) and k is the momentum of one of the particles in the πN c.m. For the kinematics and transition under consideration $\Gamma(E)\sim 50$ MeV. Pion and proton distortions have been included using parameters given in Sec. II. The results of the calculations using various widths and Δ-nucleus potential parameters are shown in Fig. 4. The results indicate that the shape of the predicted angular distributions are not appreciably effected by details of the Δ-nucleus interaction and whether the free or energy dependent width is adopted in the resonance region. For both the target and projectile emission diagrams reduction factors of ∼2 result as one changes from an energy dependent width and phenomenological Δ-nucleus interaction to a free width and no Δ-nucleus interaction. Apparently this occurs, below the resonance region, because the important *total* effective width in the delta prop-

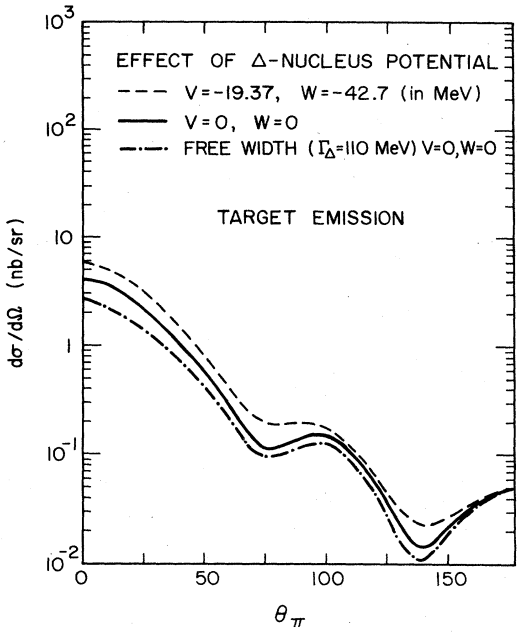

FIG. 4. Effect of the Δ-nucleus potential and Δ width on the target emission contribution to the differential cross section for the reaction $^{12}C(p,\pi^+)^{13}C_{g.s.}$ for an incident proton laboratory kinetic energy of 250 MeV.

agator is less in the former case than in the latter.

The general importance of allowing for Δ propagation is shown in Fig. 5. In this case no pion or proton distortions are included so that effects clearly associated with Δ propagation can be seen. The result shown, for the target emission diagram and the reaction $^{12}C(p,\pi^+)^{13}C_{g.s.}$, $T_p^{lab}=265$ MeV, indicates that *both* the shape of the angular distribution and the general magnitude of the differential cross section is appreciably changed by allowing propagation. The calculation including Δ propagation yields more structure and an enhancement in the differential cross section compared to the model calculation where a nonpropagating Δ is included. (The limit of the nonpropagating Δ is obtained by replacing the kinetic energy operator in the Δ propagator by a C number.)

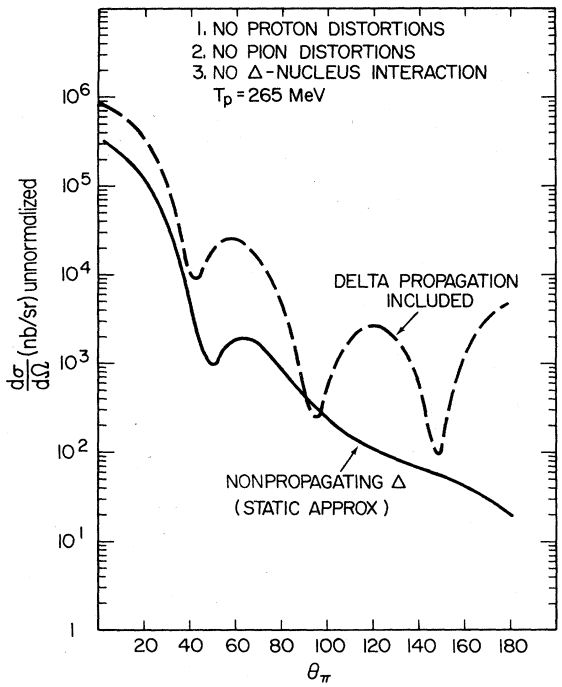

FIG. 5. The target emission contribution to the differential cross section for $^{12}C(p,\pi^+)^{13}C_{g.s.}$, $T_p^{lab}=265$ MeV when (a) (solid line) the kinetic energy term in the Δ propagator is assumed to be a C number. (b) (dashed line) the kinetic energy term is treated as an operator.

B. Sensitivity of results to proton and pion distortions and bound nucleon orbitals

Since previous SNM calculations have shown considerable sensitivity to the parameters associated with the single nucleon bound and continuum wave functions,[1] it is of interest to study the sensitivity of the TNM results to the nucleon wave functions. First consider the sensitivity of the $^{12}C(p,\pi^+)^{13}C_{g.s.}$ predictions to whether harmonic oscillator (HO) or Saxon-Woods (SW) bound nucleon orbitals are adopted. The results, shown in Fig. 6, indicate that for both the target and projectile emission diagrams the difference between using harmonic oscillator or Saxon-Woods orbitals is negligible. The Saxon-Woods parameters used for the bound orbitals were $a=a_{so}=0.53$ fm and $R=R_{so}=1.25$ fm. The well depths were varied to yield the single particle binding energies for each orbit. The relative lack of sensitivity to the orbitals in the TNM compared to the SNM may be understood by the following. In a SNM all the momentum transfer (after accounting for the distortions) is given to one nucleon (the incident nucleon which gets bound). Thus, one is exploring the wave function of the bound nucleon at large momentum transfer, Q. In momentum space the HO and SW

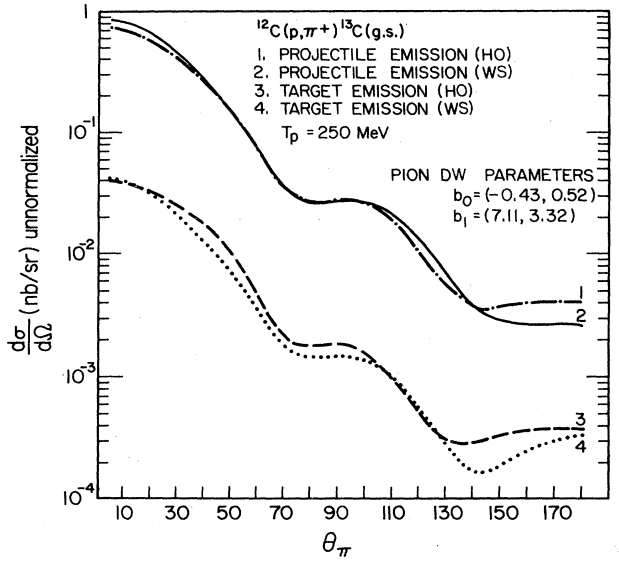

FIG. 6. The differential cross section contribution arising from projectile and target emission diagrams assuming harmonic oscillator (HO) or Saxon-Woods (SW) single nucleon bound orbitals. Full proton and pion distortions have been included.

wave functions differ considerably at large Q, resulting in a sensitivity to the bound state wave functions. In a TNM, however, the momentum Q is shared by three bound wave functions, so that one is exploring each of the wave functions in a region of smaller Q where the HO and SW wave functions have very similar form. Thus the TNM should not be as sensitive to the type of the bound state functions utilized as long as they are similar at low $Q \lesssim k_F$. This insensitivity of the TNM to the single orbital nuclear structure is very encouraging, as it paves the way to better understanding the reaction mechanism involved in pion production. Of course, the details of the many-particle nuclear structure may still be important.

Next we consider the sensitivity of the calculations to pion and proton distortions. Figure 7 illustrates the effect of pion distortions on the angular distributions for the $^{12}C(p,\pi^+)^{13}C_{g.s.}$ reaction. We see that increasing or decreasing the pion distortion potential by $\sim 10\%$ has very little effect on the angular distributions. The most striking effect is obtained, of course, by the turning off of the pion distortions. In this case we see that the angular distributions are not affected at forward angles, $\theta \lesssim 50°$. For larger angles the cross section drops smoothly and rapidly. The fact that the angular distributions do not vary appreciably for forward angles is a new feature. There is apparently no SNM which can reproduce this behavior of the angular distributions. In the SNM, turning off the pion distortions makes the angular distributions decrease by an order of magnitude. The fact that, in our model, angular distributions without any distortions do not begin to differ from those with pion distortions included (until $\theta_{c.m.} > 50°$) is a positive feature of the TNM which can be explained by the following discussion. An incoming proton with 250 MeV of kinetic energy has about 720 MeV/c momentum. For pion production on ^{12}C, exciting the low-lying states of ^{13}C, the outgoing pion has roughly 200 MeV/c momentum. Thus the momentum transferred to the nucleus is about 520 MeV/c at forward angles. In the TNM this momentum transfer is shared by the three bound state wave functions. Thus, one is exploring these wave functions for $Q \approx 170$ MeV/c momentum, which is well below the Fermi momentum (250 MeV/c). Therefore, one does not depend critically upon the pion distortions to transfer 520 MeV/c momentum to the nucleus as in the SNM. This results in the insensitivity of the angular distributions (at forward angles) to turning off and on of the pion distortions. As we begin to look at the process away from forward angles, the momentum transferred to the nucleus begins to increase. At $\theta = 180°$, $Q = 920$ MeV/c and thus each of the three wave functions is evaluated in a momentum region somewhat greater than the Fermi momentum. Hence, the pion distortions begin to play an important role in determining the effective momentum sharing. It appears from Fig. 7 that pion distortions begin to play a significant role in the momentum sharing whenever the bound nucleons have to absorb more than ~ 200 MeV/c momentum. For higher momentum transfer ($Q > 600$ MeV/c), perhaps more than two nucleons begin to take part in the pion production. Hence, if one wants to cut down the effect of the pion distortions in the model, perhaps higher-order processes (involving more than two nucleons) should be treated microscopically.

Next we consider the effect of proton distortions on the shape and magnitude of the angular distributions for the

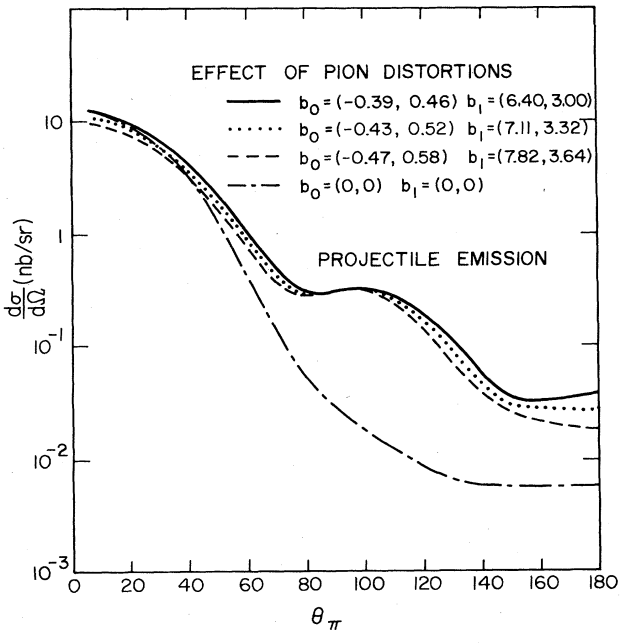

FIG. 7. The effect of pion distortions on the angular distribution for the $^{12}C(p\pi^+)^{13}C_{g.s.}$ reaction for $T_p^{lab} = 250$ MeV. Only projectile emission diagram contributions have been included. Harmonic oscillator orbitals and full proton distortions have been used in obtaining all curves shown.

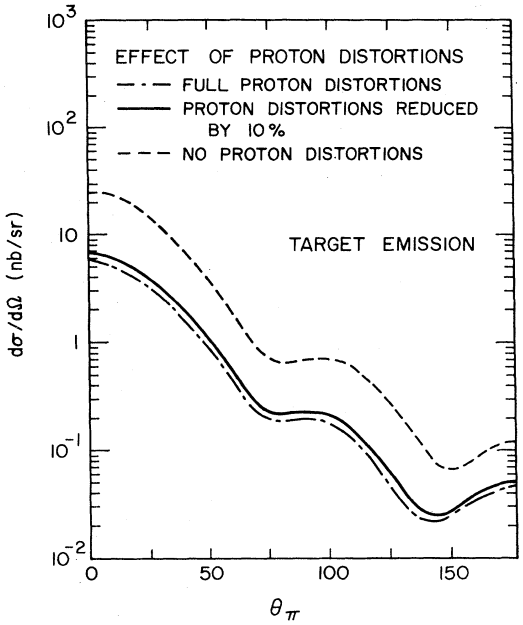

FIG. 8. The effect of proton distortions on the angular distribution for the $^{12}C(p,\pi^+)^{13}C_{g.s.}$ reaction for $T_p^{lab} = 250$ MeV. Only target emission diagram contributions have been included. Harmonic oscillator orbitals and full pion distortions have been used in obtaining all curves shown.

same transition treated above. We see from Fig. 8 that for the target emission diagram a 10% change in the proton optical potential results in approximately a 10% change in the differential cross section with the shape of the angular distribution remaining the same. Of course, a more dramatic effect is obtained by turning off the proton distortions. The differential cross section increases by a factor of 3, with the shape of the angular distributions almost unaltered. This effect shows that, in a TNM, the (p,π) reaction is quite insensitive to the proton distortions. The increase in the differential cross section obtained by decreasing the strength of the proton optical potential is merely due to the fact that one is decreasing the strength of the absorptive part of the optical potential. The fact that the shape of the angular distributions remains unchanged shows that, in a TNM, proton distortions play a minor role in the momentum sharing process (for $Q < 800$ MeV/c). In a SNM, although the dependence of the angular distributions on the proton distortions is not as severe as on the pion distortions, it is still strong.[1]

C. Studies associated with the one-boson exchange NN→NΔ transition potential

The two-body NN→NΔ transition potential has two terms for each boson [see Eq. (2)], a scalar ($\lambda_i=0$) and a tensor ($\lambda_i=2$) piece. In Fig. 9 we have shown the relative contributions from the scalar and the tensor parts of the pion transition potential for the projectile emission diagram. One sees that the tensor part of the NN→NΔ interaction is larger at all the angles by more than a factor of 2. Also notice that the scalar piece is fairly smooth. The effect of including only the ρ meson exchange poten-

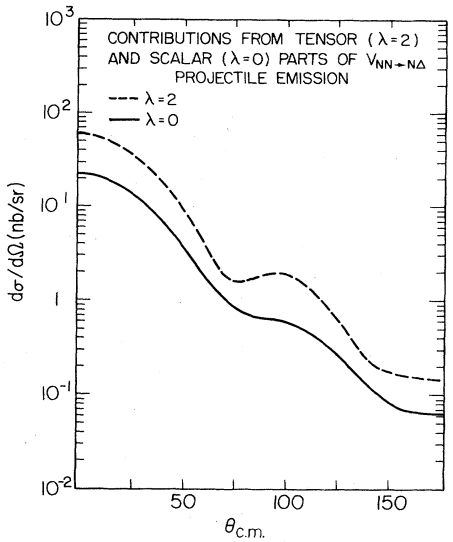

FIG. 9. Contributions of the $\lambda_i=2$ (tensor) and $\lambda_i=0$ (scalar) parts of the pion exchange potential $V_{NN\to N\Delta}$ to the differential cross section for the $^{12}C(p,\pi^+)^{13}C_{g.s.}$ reaction at $T_p^{lab}=250$ MeV. Full pion and proton distortions have been included. Harmonic oscillator orbitals have been adopted. Only the projectile emission diagram contributions have been included.

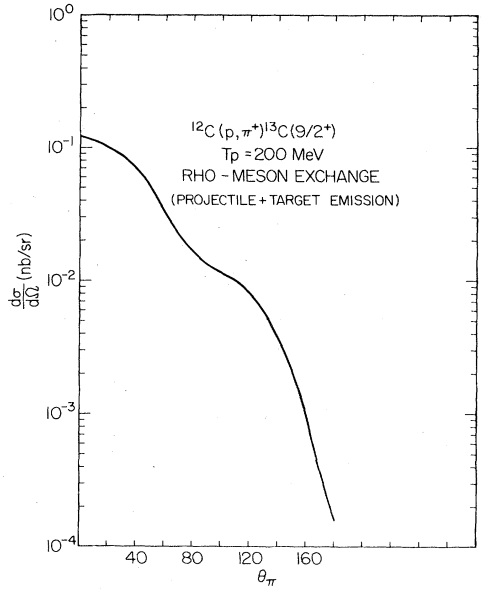

FIG. 10. The predicted differential cross section including only the rho (ρ) meson piece of the NN→NΔ transition potential. The reaction is $^{12}C(p,\pi^+)^{13}C(\frac{9}{2}^+,9.5$ MeV) for $T_p^{lab}=200$ MeV. Harmonic oscillator orbitals have been adopted and full pion and proton distortions have been included.

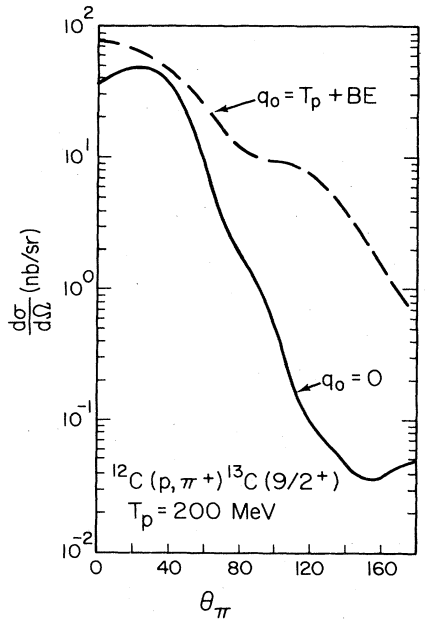

FIG. 11. Various contributions to the differential cross section for pion production in the reaction $^{12}C(p,\pi^+)^{13}C(\frac{9}{2}^+,9.5$ MeV) for $T_p^{lab}=200$ MeV. The pion contribution to the NN→NΔ transition potential and full pion and proton distortions have been included. Harmonic oscillator orbitals have been adopted. Comparison is shown of projectile (dashed line) and target (solid line) emission contributions treating a finite q_0 as discussed in Sec. II, the results of $q_0=0$ for the projectile emission piece is shown as a dot-dashed line. The term q_0 is the energy transfer appearing in the intermediate pion propagator.

tial is shown in Fig. 10 for $^{12}C(p,\pi^+)^{13}C_{g.s.}$, $T_p^{lab}=200$ MeV. We find that the few percent reduction (compared to using the pion potential only) that results when a $\rho+\pi$ transition potential is adopted occurs because of a destructive interference between the important $\lambda_i=2$ pieces of the ρ and π potentials.

As discussed in Sec. II, for low lying final nuclear states the energy term q_0 appearing in the pion propagator is only a few MeV for the target emission diagram while q_0 can be 200—300 MeV for the projectile emission contribution. We wish to point out that the q_0 term is important to include in (p,π) calculations. First note that the projectile emission diagram is dominant over a wide angular range for (p,π) reactions leading to selected final states. Therefore, in Fig. 11(b) we compare the projectile emission contribution with the q_0 term deleted in the propagator with the result obtained by setting $q_0=T_p+|E_B|_{1d_{5/2}}$. The difference is significant, resulting in an enhancement for the finite q_0 term with the enhancement increasing for larger angles. We note that the sensitivity to the type of single particle orbital adopted (see Fig. 6), or to the strength of the Δ-nucleus interaction (see Fig. 4), or to modest changes in the proton and pion optical potentials used for generating the final pion and initial proton distorted waves, respectively (see Figs. 7 and 8), is no greater than the sensitivity to keeping the q_0 term in the TNM.

D. Effect of intermediate ρ exchange

The coupling constants and mass for the intermediate ρ exchange are given in Appendix A. We find that the inclusion of an intermediate ρ exchange has a negligible effect on the differential cross section. This is in agreement with the results of Londergan and Nixon[17] and is a consequence of using single particle wave functions (for π and ρ exchange matrix elements) which tend to have relatively small high momentum components. However, we should point out that it has been shown by Arima *et al.*[18] that one may obtain different results for π and ρ exchange matrix elements if one uses nuclear wave functions containing *two-nucleon* correlations induced by the tensor force. Thus, in this latter case the effect of ρ exchange may be greater than we have found. This is an important area of future research for reaction mechanism studies involving two active nucleons.

E. Energy dependence and comparison with experiment

The predicted energy dependence of the $^{12}C(p,\pi^+)^{13}C(\frac{9}{2}^+, 9.5$ MeV) differential cross section is shown in Fig. 12(a). The results indicate a strong dependence on energy of the shape and magnitude of the angular distribution. A simple $(1d_{5/2})(1p_{1/2})(1p_{3/2})^{-1}$ 2p-1h final state (using harmonic oscillator orbitals) has been utilized for these model calculations. For this transition the projectile-emission diagram dominates, and thus the energy dependence mainly reflects the changes in this diagram's predicted angular distribution. For comparative purposes we have shown the available experimental data in Fig. 12(b). While the magnitude of the cross section is not accurately predicted (nor expected—see later discussion), the general trend of the shape and energy dependence of data is well reproduced by the TNM. Clearly data at the energy range above $T_p=250$ MeV are

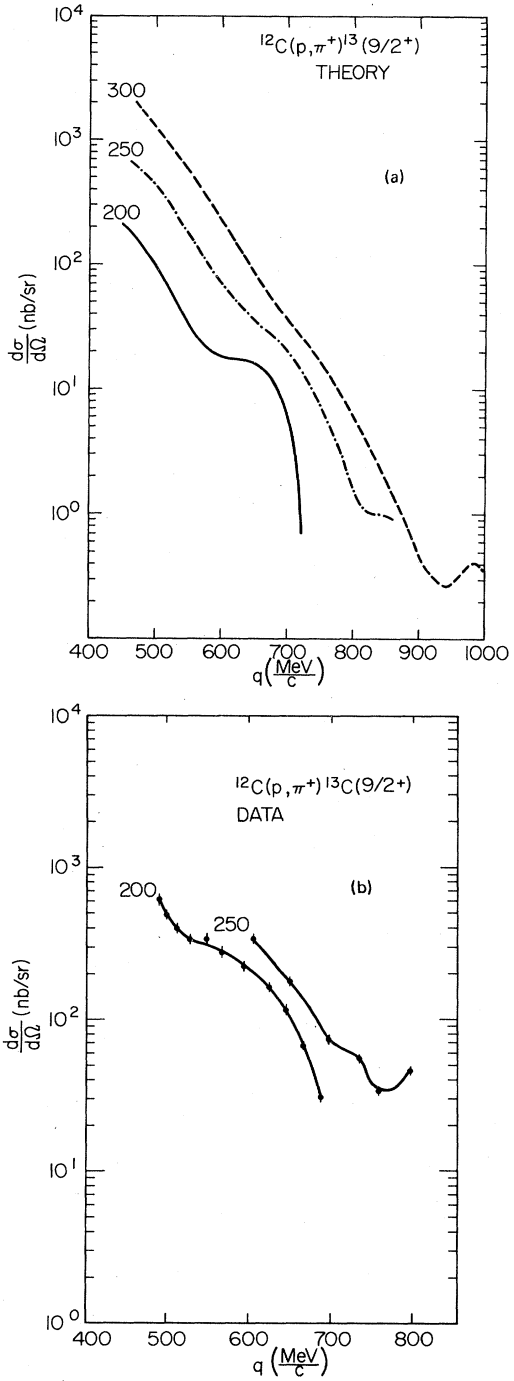

FIG. 12. (a) Predicted energy dependence of the $^{12}C(p,\pi^+)^{13}C(\frac{9}{2}^+,9.5$ MeV) reaction as given by the TNM model with a propagating Δ and full external particle distortions. The angular distributions are plotted as a function of the momentum transfer, q, to the nucleus. (b) Experimental data for the reaction shown in (a). The lines through the data are to guide the eye (Ref. 19).

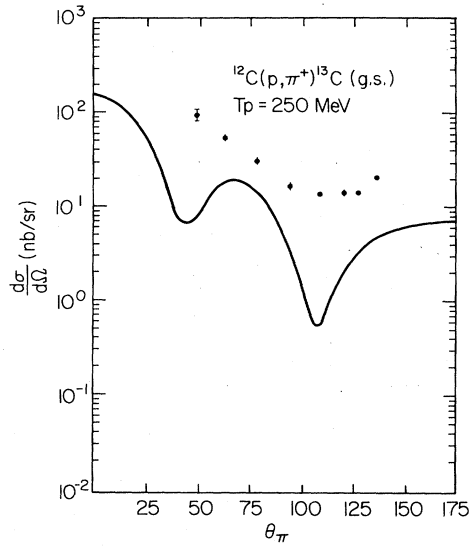

FIG. 13. Comparison between theory and experiment for the $^{12}C(p,\pi^+)^{13}C_{g.s.}$ reaction at $T_p=250$ MeV. The TNM model developed in this paper has been used in the calculation. The experimental data is from Ref. 20.

important for comparison with the model.

We show a comparison of a TNM prediction for $^{12}C(p,\pi^+)^{13}C_{g.s.}$, $T_p=250$ MeV with experimental data in Fig. 13. The theory is not in quantitative agreement with experiment, however, some features of the angular shape of the data are reproduced. The conclusion is that the TNM in its present form does not yet quantitatively fit the data but that the general shapes and energy dependence, for the transitions studied, are reasonably well predicted. We note that Keister and Kisslinger[9] find that use of more realistic wave functions for $^{13}C_{g.s.}$ results in a change in the magnitude of the $^{12}C(p,\pi^+)^{13}C_{g.s.}$ predictions while leaving the *shape* of the angular distribution substantially unchanged.

IV. SUMMARY AND CONCLUSIONS

In this initial investigation we have developed and applied a microscopic model of the pion production reaction mechanism that involves two active nucleons (TNM). The principal new feature of the present model is that it allows for propagation of an intermediate Δ resonance taking into account interactions with the many-nucleon medium. Other features of the model allow for a finite range one-meson exchange transition potential, $V_{NN\to N\Delta}$, full external pion and proton distortions, and flexibility in choosing the geometric form of the bound nucleon orbitals. Transitions to single valence particle or two-particle—one-hole final states from any of the (p,π^+), (p,π^0), or (p,π^-) reactions are treated on equal footing in the model.

Heretofore, comparison between theory and experiment has not been encouraging; the existing single nucleon mechanism (SNM) theories possess considerable sensitivity to the parameters entering in effective potentials determining bound state and distorted wave functions. Presumably a fair amount of this sensitivity originates from the fact that pion production is a high momentum transfer process, and thus, in the SNM, details of momentum space bound orbitals and distorted waves at high momentum transfer are unphysically accentuated. In a TNM with a propagating intermediate Δ the pathological high momentum dependence is alleviated by the facts that (a) there are now two active nucleons to absorb the high momentum transfer and (b) an additional momentum smearing effect is introduced by the nonlocality originating from the propagating Δ. As a result, we find for our TNM model that the results are not overly sensitive to the orbitals adopted and the distortion parameters (see Figs. 6—8). For the particular transitions we studied, the shape of the angular distributions were quite stable, at forward and medium angles, to changes in the parameters under consideration. At very large angles the momentum transfer is large enough so that *more* than two active nucleons may be required to adequately treat the reaction.

Studies of the meson exchange transition potential reveal the dominance of the tensor component of the reaction (see Fig. 9). The more realistic $\pi+\rho$ transition potential yielded a prediction similar in shape but smaller in magnitude than the π transition potential alone (see Fig. 10). One expects this to be a general result because of the destructive interference between the important tensor contributions of the two potentials. The crucial importance of including the energy transfer component in the meson propagator for the projectile emission contribution was illustrated in Fig. 11. The relative importance of the target emission and projectile emission contributions was seen to be a function of the transition and angle under consideration (see Figs. 6 and 11). For the transitions we studied the projectile emission diagram dominated except at very large angles ($\theta>130°$). The dominance of the projectile emission diagram for the $^{12}C(p,\pi^+)^{13}C_{g.s.}$ is consistent with recent TNM results obtained using a finite range transition potential.[9]

The most important new results obtained in this paper relate to the effects of allowing for intermediate Δ propagation. First, there is the indirect result that the sensitivity to the other parameters (distortions, orbitals) is less than found in previously explored TNM models. Second, allowing for Δ propagation can significantly affect predicted angular distributions (see Fig. 5). Third, the shape of the predicted angular distributions do not seem to be sensitive to the details of the assumed (local) Δ-nucleus interaction (see Fig. 4).

We have included some experimental data for comparison with the theoretical predictions. While comparison of angular shapes and the energy dependence of the (p,π) reaction is encouraging, the agreement between theory and experiment is still not satisfactory. Beyond using more realistic model nuclear wave functions there are several obvious improvements to the present model that are under current investigation. These are discussed briefly below.

Some additions to the present model which one might wish to include are the following:

(a) inclusion of nonresonant pion-nucleon scattering contributions;

(b) use of Dirac relativistic phenomenology for the active baryon wave functions;

(c) inclusion of nonstatic contributions at the meson production and absorption vertices in a nonrelativistic treatment;

(d) use of a more realistic *transition* operator $T_{NN\to N\Delta}$ as opposed to a one-meson exchange *potential* $V_{NN\to N\Delta}$ and/or allowing for the intermediate exchanged meson to propagate including nuclear medium effects;

(e) adoption of pion distorted waves arising from more realistic momentum space optical potentials;

(f) inclusion of pieces of the SNM not included in the present TNM; and

(g) inclusion of preemission diagrams.

As mentioned earlier, we have already completed initial studies of a microscopic TNM model for including nonresonant S and P wave pion-nucleon scattering in the present model. While this is the subject of a future presentation, we have found that, for $T_p^{lab} > 200$ MeV, the nonresonant background contribution is negligible compared to the terms already included in the present TNM model. Thus (a) above does not appear to have the potential to substantially change angular distributions in the region $200 < T_p^{lab} < 400$ MeV.

The fact that the TNM requires evaluation of nucleon wave functions below the Fermi momentum argues that (b) and (c) above may not be of crucial importance—however, detailed calculations are required to substantiate this conjecture. The fact that relativistic approaches may introduce an effective mass (due to the large scalar potential) certainly could effect predicted magnitudes of cross sections.

Contributions (d)—(g) all seem to have some potential for changing angular distributions. Additions (d), (e), and (g), while adding some computational complexity to the already formidable calculational task, are straightforward conceptually, and their inclusion will be pursued. Inclusion of the standard plane wave external pion and proton SNM is straightforward to add to the present calculation. However, Keister, and Kisslinger[9] have argued that this contribution is largely cancelled by an exchange plane wave contribution which we have also not included. Estimation of this latter term is less straightforward.

It would be useful to have more experimental data in the region above 200 MeV. This is an energy region naturally accessible to TRIUMF. At this stage differential cross section angular distributions associated with the more selective (p,π^-) reaction (where the SNM does not naturally contribute) would be the best test of the present model. Comparison of the present model with higher energy (p,π^-) data to discrete final states as well as in the continuum region would allow one to better separate better reaction mechanism and nuclear structure uncertainties.

We have not discussed analyzing power predictions in this paper and, in fact, have not yet completed such calculations. Obviously, comparison of predictions with existing asymmetry data is a stringent test of a proposed theory and will be pursued in future investigations.

APPENDIX A: TWO-BODY TRANSITION POTENTIAL $V(\mathbf{r}_1,\mathbf{r}_2)$

A. Intermediate pion

The interaction Hamiltonian at the $NN\pi$ vertex is taken to be of the static form

$$V_{NN\pi}=(f_\pi/m)\boldsymbol{\sigma}\cdot\boldsymbol{\nabla}_\pi\boldsymbol{\tau}\cdot\boldsymbol{\Phi}\ , \tag{A1}$$

where $m\equiv m_\pi$. We use a static approximation to keep the calculations tractable. Higher-order corrections to $V_{NN\pi}$ can be incorporated in the model later on. Here $\boldsymbol{\nabla}_\pi$ is the derivative operator acting on the pion wave function $\boldsymbol{\Phi}$. The pion-nucleon coupling strength, f_π, is $\sqrt{4\pi\times 0.088}$. The matrix representations of the operators connecting two-component spinors in spin and isospin spaces are $\boldsymbol{\sigma}$ and $\boldsymbol{\tau}$, respectively. The pion wave function, $\boldsymbol{\Phi}$, is a scalar in spin space and vector in isospin space.

The static form for the $\Delta N\pi$ interaction Hamiltonian can similarly be written as

$$V_{\Delta N\pi}=(f_\pi^*/m)\mathbf{S}^\dagger\cdot\boldsymbol{\nabla}_\pi\mathbf{T}^\dagger\cdot\boldsymbol{\Phi}\ . \tag{A2}$$

Here the S (T) are 4×2 matrix representations of the operators connecting spin (isospin) $\frac{3}{2}$ states with spin (isospin) $\frac{1}{2}$ states, and f_π^* is the $\Delta N\pi$ coupling strength. In the quark model f_π^* is related to f_π through $SU(2)_{spin}\times SU(2)_{isospin}$ symmetry by

$$f_\pi^*=\sqrt{(72/25)}f_\pi\ .$$

In momentum space we assume the two-body transition potential, generated by one-pion exchange, to be

$$V(\mathbf{r}_1,\mathbf{r}_2)=(2\pi)^{-3}\int_0^\infty d\mathbf{q}\exp[i\mathbf{q}\cdot(\mathbf{r}_1-\mathbf{r}_2)]V(\mathbf{q})\ , \tag{A3}$$

where

$$V(\mathbf{q})=-(f_\pi/m)(f_\pi^*/m)[(\Lambda^2-m^2)/(\Lambda^2-q_\mu^2)]^2 \times\boldsymbol{\sigma}_1\cdot\mathbf{q}\mathbf{S}_2\cdot\mathbf{q}\boldsymbol{\tau}_1\cdot\mathbf{T}_2\frac{1}{q_\mu^2-m^2+i\epsilon}\ . \tag{A4}$$

In Eq. (A4), $(q_\mu^2-m^2+i\epsilon)^{-1}$ is the nonstatic pion propagator and $(\Lambda^2-m^2)/(\Lambda^2-q_\mu^2)$ is the monopole form factor at the $NN\pi$ and $\Delta N\pi$ vertices. We use a hard form factor ($\Lambda=10m_\pi$, implying a small interaction distance in configuration space) for both the $NN\pi$ and $\Delta N\pi$ vertices, as motivated by the work of Holinde, Phys. Rep. **68**, 122 (1981). Our studies indicate that the results are insensitive to small variations in Λ for $\Lambda > 1.2$ GeV.

$$\boldsymbol{\sigma}_1\cdot\mathbf{q}\mathbf{S}_2\cdot\mathbf{q}=\tfrac{1}{3}(3\boldsymbol{\sigma}_1\cdot\mathbf{q}\mathbf{S}_2\cdot\mathbf{q}-\boldsymbol{\sigma}_1\cdot\mathbf{S}_2q^2+\boldsymbol{\sigma}_1\cdot\mathbf{S}_2q^2) =\tfrac{1}{3}[S_{12}(q)+\boldsymbol{\sigma}_1\cdot\mathbf{S}_2q^2]\ , \tag{A5}$$

where $S_{12}(q)$ is defined by

$$S_{12}(q)=3\sqrt{5}[[\sigma_1\otimes S_2]^2\otimes[q\otimes q]^2]^{00}\ . \tag{A6}$$

It can be shown that

$$\boldsymbol{\sigma}_1\cdot\mathbf{q}\mathbf{S}_2\cdot\mathbf{q}=\tfrac{1}{3}\sum_{\lambda=0,2}C_\lambda^\pi(q)[Y_\lambda(\hat{\mathbf{q}})\otimes[\sigma_1\otimes S_2]^\lambda]^{00}\,, \tag{A7}$$

where

$$C_0^\pi(q)=-\sqrt{(12\pi)}q^2\,,$$
$$C_2^\pi(q)=\sqrt{(24\pi)}q^2\,. \tag{A8}$$

Thus one can write

$$V(\mathbf{r}_1-\mathbf{r}_2)=-(2\pi)^{-3}(\tfrac{1}{3})(f_\pi/m)(f_\pi^*/m)\sum_\lambda\int_0^\infty G(\Lambda,q)D_\pi(q)C_\lambda(q)\exp[i\mathbf{q}\cdot(\mathbf{r}_1-\mathbf{r}_2)][Y_\lambda(\hat{\mathbf{q}})\otimes[\sigma_1\otimes S_2]^\lambda]^{00}\,, \tag{A9}$$

where

$$G(\Lambda,q)\equiv(\Lambda^2-m^2)/(\Lambda^2-q_0^2+q^2)^2\,, \tag{A10}$$

and $D_\pi(q)$ stands for the pion propagator.

Consider the term

$$I_0=\exp[i\mathbf{q}\cdot(\mathbf{r}_1-\mathbf{r}_2)][Y_\lambda(\hat{\mathbf{q}})\otimes[\sigma_1\otimes S_2]^\lambda]^{00}\,. \tag{A11}$$

Using the partial wave expansion for the plane wave

$$\exp i\mathbf{q}\cdot\mathbf{r}=4\pi\sum_{l,m}i^l j_l(qr)Y_{lm}(\hat{\mathbf{r}})Y_{lm}^*(\hat{\mathbf{q}}) \tag{A12}$$

and

$$Y_{lm}^*(-\hat{\mathbf{q}})=(-1)^l Y_{lm}(\hat{\mathbf{q}})\,, \tag{A13}$$

one can write

$$I_0=(4\pi)^{3/2}\sum_{\lambda_1,\lambda_2,\lambda,L}(i)^{-\lambda_1+\lambda_2}(-1)^{\lambda_2+\lambda+L+1}\hat{\lambda}_1\hat{\lambda}_2\hat{\lambda}\hat{L}j_{\lambda_1}(qr_1)j_{\lambda_2}(qr_2)\begin{Bmatrix}\lambda_1&\lambda_2&\lambda\\0&0&0\end{Bmatrix}\begin{Bmatrix}\lambda_1&\lambda_2&\lambda\\1&1&L\end{Bmatrix}$$
$$\times[[Y_{\lambda_1}(\hat{\mathbf{r}}_1)\otimes\sigma_1]^L\otimes[Y_{\lambda_2}(\hat{\mathbf{r}}_2)\otimes S_2]^L]^{00} \tag{A14}$$

where the abbreviation $x=\sqrt{(2x+1)}$ has been used. The large parentheses and curly bracketed expressions are the usual $3J$ and $6J$ symbols, respectively, defined in Ref. 11. One thus can write the two-body transition potential in partial wave decomposed form as

$$V(\mathbf{r}_1-\mathbf{r}_2)=\sum_{\lambda_1,\lambda_2,\lambda,L}E_{\lambda_1\lambda_2\lambda L}\int_0^\infty q^2G(\Lambda,q)C_\lambda^\pi(q)D_\pi(q)j_{\lambda_1}(qr_1)j_{\lambda_2}(qr_2)[[Y_{\lambda_1}(\hat{\mathbf{r}}_1)\otimes\boldsymbol{\sigma}_1]^L\otimes[Y_{\lambda_2}(\hat{\mathbf{r}}_2)\otimes\mathbf{S}_2]^L]^{00}\,, \tag{A15}$$

where we have defined

$$E_{\lambda_1\lambda_2\lambda L}=-(3\pi)^{-3/2}(f_\pi/m)(f_\pi^*/m)(i)^{-\lambda_1+\lambda_2}(-1)^{\lambda_2+\lambda+L+1}\hat{\lambda}_1\hat{\lambda}_2\hat{\lambda}\hat{L}\begin{Bmatrix}\lambda_1&\lambda_2&1\\0&0&0\end{Bmatrix}\begin{Bmatrix}\lambda_1&\lambda_2&\lambda\\1&1&L\end{Bmatrix}. \tag{A16}$$

B. Intermediate rho meson

If the intermediate boson is a rho meson then Eq. (A4) is modified to the form

$$V_\rho(q)=\frac{f_\rho}{m_\rho}\frac{f_\rho^*}{m_\rho}[(\Lambda^2-m^2)/(\Lambda^2+q_u^2)]^2$$
$$\times\frac{(q^2\boldsymbol{\sigma}_1\cdot\mathbf{S}_2-\boldsymbol{\sigma}_1\cdot\mathbf{q}\mathbf{S}_2\cdot\mathbf{q})}{q_\mu^2-m_\rho^2+i\epsilon}\boldsymbol{\tau}_1\cdot\mathbf{T}_2\,, \tag{A17}$$

where

$$\frac{f_\rho}{m_\rho}\equiv\frac{g_{\mathrm{NN}\rho}}{2m}\frac{(1+f_{\mathrm{NN}\rho})}{g_{\mathrm{NN}\rho}}=0.593$$

and

$$\left[\frac{f_\rho}{m_\rho}\right]^*=\left[\frac{72}{25}\right]^{1/2}\left[\frac{f_\rho}{m_\rho}\right]=1.006\,.$$

Now using the result that

$$q^2\boldsymbol{\sigma}_1\cdot\mathbf{S}_2-\boldsymbol{\sigma}_1\cdot\mathbf{q}\mathbf{S}_2\cdot\mathbf{q}$$
$$=\tfrac{1}{3}\sum_{\lambda=0,2}C_\lambda^\rho(q)[Y_\lambda(\hat{\mathbf{q}})\otimes[\sigma_1\otimes S_2]^\lambda]^{00} \tag{A18}$$

where

$$C_0^\rho=2C_0^\pi=-2\sqrt{(12\pi)}q^2 \tag{A19a}$$

and

$$C_0^\rho=-C_2^\pi=-\sqrt{(24\pi)}q^2\,, \tag{A19b}$$

the two-body transition potential for the intermediate ρ meson is given by Eq. (A15) if C_λ^π is replaced by C_λ^ρ, $D_\pi(q)$ is replaced by $D_\rho(q)$, and, in $E_{\lambda_1\lambda_2\lambda L}$, $(f_\pi/m_\pi)(f_\pi^*/m_\pi)$ is replaced by $(f_\rho/m_\rho)(f_\rho^*/m_\rho)$. We adopt the same form factor for the ρ coupling as for the π coupling.

C. Formation of the initial state

We expand the proton distorted wave as

$$\Psi_{m_{s_1}}(\mathbf{k}_p,\mathbf{r})=\sum_{m_{s_2}}\Psi_{m_{s_1},m_{s_2}}(\mathbf{k}_p,\mathbf{r})\chi_{m_{s_2}}$$
$$=(4\pi/k_p)\sum_{\substack{j_1,l_1,m_{l_1}\\M_1}}(i)^{l_1}\exp(i\sigma_{l_1})U_{l_1j_1}(k_p,r)r^{-1}(l_1m_{l_1}\tfrac{1}{2}m_{s_1}\,|\,j_1M_1)$$
$$\times(l_1m'\tfrac{1}{2}m_{s_2}\,|\,j_1M_1)Y^*_{l_1m_{l_1}}(\hat{\mathbf{k}}_p)Y_{l_1m'}(\hat{\mathbf{r}})\chi_{m_{s_2}}\,, \tag{A20}$$

where $m'=m_{l_1}+m_{s_1}-m_{s_2}$. In Eq. (A20), $U_{l_1j_1}$ is the radial part of the proton distorted wave, σ_{l_1} is the phase shift for the lth particle wave, and χ_{m_s} is the spin part of the proton wave function.

Using the result

$$Y_{l_1m'}(\hat{\mathbf{r}})\chi_{m_{s_1}}=\sum_{j_1,M_3}(l_1m'\tfrac{1}{2}m_{s_1}\,|\,j_1M_3)[Y_{l_1}(\hat{\mathbf{r}})\otimes\tfrac{1}{2}]^{j_1M_3}\,, \tag{A21}$$

we can write

$$\Psi_{m_{s_1}}(\mathbf{k}_p,\mathbf{r})=(4\pi/k_pr)\sum_{j_1,l_1m_{l_1},M_1}(i)^{l_1}\exp(i\sigma_{l_1})(-1)^{-l_1-M_1+1/2}\hat{\mathrm{j}}_1U_{l_1j_1}(k_p,r)$$
$$\times\begin{pmatrix}l_1 & \frac{1}{2} & j_1\\ M_{l_1} & M_{s_1} & -M_1\end{pmatrix}Y^*_{l_1m_{l_1}}(\hat{\mathbf{k}}_p)[Y_{l_1}(\hat{\mathbf{r}})\otimes\tfrac{1}{2}]^{j_1M_1}\,. \tag{A22}$$

We can rewrite the closed shell as a particle in a state $|j_2'm_2'\rangle$ coupled to rest of the nucleus, which itself is represented as a hole in the state $|j_2'm_2'\rangle$. Then the nuclear ground state can be written as (suppressing isospin variables)

$$|0^+\rangle=\sum_{j_2}(1/\hat{j}_2')[j_2'\bar{j}_2']^{00}\,,$$

where the factor $(1/\hat{j}_2')$ is included to properly normalize the particle-hole state. The total initial state, a proton coupled to a closed shell $J=0$ $J_z=0$ nucleus, can be written as

$$|\,\text{initial}\rangle=\Psi_{m_{s_1}}(\mathbf{k}_p,\mathbf{r})\,|0^+\rangle\,. \tag{A23}$$

A simple exercise in angular momentum coupling then leads to the result

$$|\,\text{initial}\rangle=\sum_{\substack{m_{l_1},M_1,j_2,\\ l_1,j_1,j_{12}}}C_0[[j_1\otimes j_2']^{J_{12}}\otimes\bar{j}_2']^{j_1M_1}\,, \tag{A24}$$

where

$$C_0\equiv(4\pi/k_p)(i)^{l_1}(-1)^{-l_1+1/2-M_1+j_1+j_{12}+j_2'}\hat{j}_{12}(\hat{j}_2')^{-2}$$
$$\times\exp(i\sigma_{l_1})\begin{pmatrix}l_1 & \frac{1}{2} & j_1\\ m_{l_1} & m_{s_1} & -M_1\end{pmatrix}Y^*_{l_1m_{l_1}}(\hat{\mathbf{k}}_p)\,. \tag{A25}$$

$U_{l_1j_1}(k_p,r)$ has been absorbed in the definition of state j_1.

D. Formation of the intermediate state

The intermediate state consists of a $\Delta(1236)$, a nucleon particle, and a nucleon hole. We form the intermediate state by first coupling the Δ and the nucleon to some total angular momentum, J, and z component, J_z, and then coupling this Δ-nucleon particle state with the remaining nucleon-hole state. A bound-state wave function is written

$$\Phi_{nljM}(\mathbf{r})=\sum_{m_lm_s}R_{nlj}(r)Y_{lm_l}(\hat{\mathbf{r}})\chi_{m_s}(lm_l\tfrac{1}{2}m_s\,|\,jM)\,, \tag{A26}$$

and the intermediate state in a jj coupling scheme is defined via

$$|\,\text{intermediate}\rangle=\sum_{j_3}\alpha[[j_\Delta\otimes j_2]^{j_3}\otimes\bar{j}_2']^{J_0M_0}\,, \tag{A27}$$

where α is a normalization constant. Using the expressions given above, after some angular momentum algebra, the matrix elements of $V(\mathbf{r}_1-\mathbf{r}_2)$ between initial and final states can be written

$$\langle \text{intermediate} \mid V(\mathbf{r}_1-\mathbf{r}_2) \mid \text{initial} \rangle$$

$$= \sum_{i=1,2} \sum_{\substack{M_1 J_1 l_1 \\ J_2 J_{12}}} \sum_{\substack{\lambda_1 \lambda_2 \\ \lambda_1 L}} \alpha C_0 E^i_{\lambda_1 \lambda_2 L} \int_0^\infty q^2 G(\Delta,q) D_i(q) C_{\lambda i}(q) dq (\sqrt{6/2\pi})(-1)^{j_2+j_1+L+l_2+l_\Delta+1}$$

$$\times \hat{j}_2 \hat{j}_1 \hat{l}_2 \hat{l}_1 \hat{\lambda}_1 \hat{j}_\Delta \hat{j}'_2 \hat{L} \hat{l}_\Delta \hat{\lambda}_2 \hat{l}'_2 \begin{bmatrix} l_2 & \lambda_1 & l_1 \\ 0 & 0 & 0 \end{bmatrix} \begin{bmatrix} l_\Delta & \lambda_2 & l'_2 \\ 0 & 0 & 0 \end{bmatrix}$$

$$\times \begin{Bmatrix} j_2 & j_1 & L \\ j'_2 & j_\Delta & j_3 \end{Bmatrix} \begin{Bmatrix} l_2 & l_1 & \lambda_1 \\ \frac{1}{2} & \frac{1}{2} & 1 \\ j_2 & j_1 & L \end{Bmatrix} \begin{Bmatrix} l_\Delta & l'_2 & \lambda_2 \\ \frac{3}{2} & \frac{1}{2} & 1 \\ j_\Delta & j'_2 & L \end{Bmatrix}$$

$$\times \int_0^\infty r_1^2 R_{n_2 l_2 j_2}(r_2) r_1^{-1} j_\lambda(q r_1) U_{l_1,j_1}(k_p, r_1) r_1^{-1} dr_1$$

$$\times \int_0^\infty r_2^2 R_{n_\Delta l_\Delta j_\Delta}(r_2) j_{\lambda_2}(q r_2) R_{n'_2 l'_2 j'_2}(r_2) r_2^{-1} dr_2 \ , \tag{A28}$$

where $i=1$ (2) denotes the pion (rho) transition potential matrix element and the bracketed expression containing nine angular momentum labels is the $9j$ symbol defined in Ref. 11. Note that in obtaining Eq. (A28) we have utilized a function $\delta_{J_0,j_1}\delta_{M_0,m_1}$ resulting from the fact that V is a scalar transition operator for the entire baryonic system.

APPENDIX B: ONE-BODY TRANSITION POTENTIAL $V(\mathbf{r}_3)$

The static one-body transition potential at the $\Delta N\pi$ vertex involving the external pion can be written as

$$V(\mathbf{r}_3) = -(f^*_\pi/m)\mathbf{S}_2^\dagger \cdot \nabla_\pi \Phi^{(-)*}(\mathbf{k}_\pi, \mathbf{r}_3) \mathbf{T}_2^\dagger \cdot \boldsymbol{\phi} \ . \tag{B1}$$

Here $\Phi^{(-)*}(\mathbf{k}_\pi, \mathbf{r}_3)$ is the pion distorted wave with outgoing boundary conditions. The symbol $\boldsymbol{\phi}$ denotes the pion wave function in isospin space. A partial wave decomposition for the pion distorted wave can be written in the form

$$\Phi^{(-)*}(\mathbf{k}_\pi, \mathbf{r}_3) = (4\pi/k_\pi) \sum_{l_\pi, m_\pi} (i)^{-l_\pi} \exp(i\sigma_{l_\pi}) \frac{\Phi_{l_\pi}(k_\pi, r_3)}{r_3} Y_{l_\pi m_\pi}(\hat{\mathbf{r}}_3) Y^*_{l_\pi m_\pi}(\hat{\mathbf{k}}_\pi) \ . \tag{B2}$$

Let us consider the term $\mathbf{S}_2^\dagger \cdot \nabla_\pi \Phi^{(-)*}(\mathbf{k}_\pi, \mathbf{r}_3)$. We use the identity

$$\nabla \psi_l(r) Y_{lm}(\mathbf{r}) = -\sqrt{(l+1)/(2l+1)}(d/dr - l/r)\psi_l(r) \underline{Y}_{l,l+1,m}(\hat{\mathbf{r}}) + \sqrt{l/(2l+1)}[d/dr + (l+1)/r]\psi_l(r) \underline{Y}_{l,l-1,m}(\hat{\mathbf{r}}) \ , \tag{B3}$$

where the $\underline{Y}_{JlM}(r)$ are the usual vector spherical harmonics

$$Y_{JlM}(\hat{\mathbf{r}}) = \sum_{m,q} Y_{lm}(\hat{\mathbf{r}}) \mathbf{e}_q (lm\,1q \mid JM) \ , \tag{B4}$$

and where the $\mathbf{e}_q$ are spherical unit vectors defined in terms of unit vectors in rectangular coordinates $\mathbf{e}_x$, $\mathbf{e}_y$, and $\mathbf{e}_z$ as

$$\mathbf{e}_+ = -1/\sqrt{2}(\mathbf{e}_x + \mathbf{e}_y), \quad \mathbf{e}_0 = \mathbf{e}_z, \quad \mathbf{e}_- = 1/\sqrt{2}(\mathbf{e}_x - i\mathbf{e}_y) \ . \tag{B5}$$

The e_q satisfy the following relations:

$$\mathbf{e}^*_q = (-1)^q \mathbf{e}_{-q}, \quad \mathbf{e}^*_q \cdot \mathbf{e}'_q = (-1)^q \mathbf{e}_q \cdot \mathbf{e}'_q = \delta'_{q,q} \ . \tag{B6}$$

Utilizing Eqs. (B1)—(B6), $V(\mathbf{r}_3)$ can be written (suppressing isospin variables)

$$V(\mathbf{r}_3) = -(f^*_\pi/m)(4\pi/k_\pi) \sum_{l_\pi m_\pi} (i)^{-l_\pi} \exp(i\sigma_{l_\pi}) Y^*_{l_\pi m_\pi}(\hat{\mathbf{k}}_\pi)$$

$$+ [\alpha_{l_\pi}(k_\pi, r_3)/r_3 [Y_{l_\pi+1}(\hat{\mathbf{r}}_3) \otimes S_2^\dagger]^{l_\pi m_\pi} + \beta_{l_\pi}(k_\pi, r_3)/r_3 [Y_{l_\pi-1}(\hat{\mathbf{r}}_3) \otimes S_2^\dagger]^{l_\pi m_\pi}] \ , \tag{B7}$$

where α_{l_π} and β_{l_π} are defined by

$$\alpha_{l_\pi} \equiv \alpha_{l_\pi}(k_\pi, r_3) = -\sqrt{(l_\pi+1)/(2l_\pi+1)}[d/dr_3 - (l_\pi+1)/r_3]\Phi_{l_\pi}(k_\pi, r_3) \ , \tag{B8a}$$

$$\beta_{l_\pi} \equiv \beta_{l_\pi}(k_\pi, r_3) = \sqrt{l_\pi/(2l_\pi+1)}(d/dr_3 + l_\pi/r_3)\Phi_{l_\pi}(k_\pi, r_3) \ . \tag{B8b}$$

One can absorb α_{l_π} and β_{l_π} in the definitions of $Y_{l_\pi+1}$ and $Y_{l_\pi-1}$, respectively, and write $V(\mathbf{r}_3)$ in abbreviated form as

$$V(\mathbf{r}_3)=\sum_{l_\pi,m_\pi} F_{l_\pi m_\pi}[[Y_{l_\pi+1}(\mathbf{r}_3)\otimes S_2^\dagger]^{l_\pi m_\pi} +[Y_{l_\pi-1}(\mathbf{r}_3)\otimes S_2^\dagger]^{l_\pi m_\pi}] , \tag{B9}$$

where

$$F_{l_\pi m_\pi}\equiv -(f_\pi^*/m)(4\pi/k_\pi) \times(i)^{-l_\pi}\exp(i\sigma_{l_\pi})Y^*_{l_\pi m_\pi}(\hat{\mathbf{k}}_\pi) . \tag{B10}$$

We reconstruct the 2p-1h final state by coupling the two particles together to give a definite angular momentum J and z projection, J_z. This two particle state is then coupled to the hole state to yield a total J_f,M_f. Thus the angular momentum coupling for the final state wave function is written

$$|\ \text{final}\rangle=\sum_{j_{24}}\epsilon[[j_4\otimes j_2]^{j_{24}}\otimes\bar{j}'_2]^{J_fM_f} , \tag{B11}$$

where ϵ is the normalization constant for the final state.

The matrix elements of the one-body transition potential between the intermediate and final states can then be written as

$$\langle\ \text{final}\ |\ V(\mathbf{r}_3)\ |\ \text{intermediate}\rangle=\sum_{j_{24}}\sum_{l_\pi,m_\pi}\epsilon\alpha F_{l_\pi,m_\pi}\langle[[j_4\otimes j_2]^{j_{24}}\otimes\bar{j}'_2]^{J_fM_f}\,|\,[Y_{l_\pi+1}(\mathbf{r}_3)\otimes S_2^\dagger]^{l_\pi m_\pi} +[Y_{l_\pi-1}(\mathbf{r}_3)\otimes S_2^\dagger]^{l_\pi m_\pi}\,|\,[[j_\Delta j_2]^{j_3}\bar{j}'_2]^{j_1M_1}\rangle . \tag{B12}$$

After some angular momentum algebra one obtains,

$$\begin{aligned}&\langle\ \text{final}\ |\ V(\mathbf{r}_3)\ |\ \text{intermediate}\rangle\\ &=\sum_{l_\pi,m_\pi}\sum_{j_{24}}\alpha\epsilon F_{l_\pi m_\pi}1/\sqrt{\pi}(-1)^{J_f-M_f+j_{24}+j'_2+j_1+j_4+j_2+j_3+l_4}\hat{j}_1\hat{J}_f\hat{j}_{24}\hat{j}_3\hat{j}_4\hat{j}_\Delta\hat{l}_\pi\hat{l}_4\\ &\times\hat{l}_\Delta\begin{bmatrix}J_f & l_\pi & j_1\\ -M_f & m_\pi & M_1\end{bmatrix}\begin{Bmatrix}j_{24} & J_f & j_2\\ j_1 & j_3 & l_\pi\end{Bmatrix}\begin{Bmatrix}j_4 & j_{24} & j_2\\ j_3 & j_\Delta & l_\pi\end{Bmatrix}\\ &\times\int_0^\infty r_3^2R_{n_\Delta l_\Delta j_\Delta}(r_3)R_{n_4l_4j_4}(r_3)r_3^{-1}dr_3\sqrt{2l_\pi+3}\begin{bmatrix}l_4 & l_\pi+1 & l_\Delta\\ 0 & 0 & 0\end{bmatrix}\begin{Bmatrix}l_4 & l_\Delta & l_\pi+1\\ \frac{1}{2} & \frac{3}{2} & 1\\ j_4 & j_\Delta & l_\pi\end{Bmatrix}\\ &\times\alpha_{l_\pi}(k_\pi,r_3)r_3^{-1}+\sqrt{2l_\pi-1}\begin{bmatrix}l_4 & l_\pi-1 & l_\Delta\\ 0 & 0 & 0\end{bmatrix}\begin{Bmatrix}l_4 & l_\Delta & l_{\pi-1}\\ \frac{1}{2} & \frac{3}{2} & 1\\ j_4 & j_\Delta & l_\pi\end{Bmatrix}\beta_{l_\pi}(k_\pi,r_3)r_3^{-1} .\end{aligned} \tag{B13}$$

APPENDIX C: DELTA PROPAGATION IN THE NUCLEAR ENVIRONMENT

The brief treatment below assumes the reader is familiar with the discussion of Δ propagation given in Ref. 12. The effective wave function for a Δ, formed from a bound nucleon and a pion, can be written as

$$\chi_{\Delta N}(\mathbf{r},\mathbf{k}_i,\omega)=\int_0^\infty d\mathbf{r}'G_\Delta(\mathbf{r},\mathbf{r}',\omega)\phi_N(\mathbf{r}')\exp(i\mathbf{k}_i\cdot\mathbf{r}') , \tag{C1}$$

where k_i is the pion momentum, ω is its energy, and $\phi_N(r')$ is the nucleon bound state wave function. The Δ propagation $G_\Delta(\gamma,\gamma',\omega)$ satisfies the following differential equation:

$$[-T_\Delta+(M+\omega-M_\Delta)+(i/2)\Gamma_\Delta(E_\Delta)-\Sigma_\Delta]G_\Delta(\mathbf{r},\mathbf{r}',\omega)=\delta(\mathbf{r}-\mathbf{r}') . \tag{C2}$$

In the above equation $E_\Delta=M+\omega+T_\Delta$, where T_Δ is the kinetic energy operator of the Δ and $M+\omega$ is the energy of the pion nucleon system in the pion-nucleus center of mass (ACM). Expanding Γ_Δ to first order in T_Δ, (C2) can be written as

$$\{-T_\Delta[1+(i/2)\Gamma'_\Delta(M+\omega)]+M+\omega-M_\Delta+(i/2)\Gamma_\Delta(M+\omega)-\Sigma_\Delta(\mathbf{r},\mathbf{r}',\omega)\}^*G_\Delta(\mathbf{r},\mathbf{r}',\omega)=\delta(\mathbf{r}-\mathbf{r}') , \tag{C3}$$

where we have defined

$$\Gamma'_\Delta(M+\omega)=\left.\frac{d\Gamma_\Delta}{dE}\right|_{E=M+\omega} . \tag{C4}$$

Using (C4) one can see that $\chi_{\Delta N}$ satisfies the following differential equation:

$$\{-T_\Delta[1+(i/2)\Gamma'_\Delta(M+\omega)]+M+\omega-M_\Delta+(i/2)\Gamma_\Delta(M+\omega)-\Sigma_\Delta(\mathbf{r},\mathbf{r}',\omega)\}\chi_{\Delta N}(\mathbf{r},\mathbf{k}_i,\omega)=\phi_N(\mathbf{r})\exp(i\mathbf{k}_i\cdot\mathbf{r}) . \tag{C5}$$

Equation (C5) is a local equation only if Σ_Δ represents a local interaction. Some of the effects giving rise to Σ_Δ (e.g., Pauli-exclusion, true pion absorption, etc.) are nonlocal in nature. However, the same situation exists in the case of the nucleon-nucleus interaction where a local potential assumption has been most often adequate. In the same spirit the Δ-nucleus potential is represented by a local potential proportional to the nuclear density, so that we have

$$\Sigma_\Delta \rightarrow (V+iW)[\rho(r)/\rho(0)] . \quad \text{(C6)}$$

Here $\rho(r)$ describes the nucleon density at a distance r from the nuclear center. V and W are the real and imaginary strengths of the Δ-nucleus interaction. Values of V and W used can be calculated from the following expression:

$$(V+iW)/T_R = a + b(E_{\pi,L}/T_R) + c(E_{\pi,L}/T_R)^2 , \quad \text{(C7)}$$

where $E_{\pi,L}$ is the kinetic energy of the pion in the laboratory and T_R is a reference value for energy. With the choice $T_R = 180$ MeV, a, b, and c, are found to be[12]

$$a = 0.44 - i0.77 ,$$

$$b = -1.24 + i1.24 ,$$

$$c = 0.47 - i0.47 .$$

This ansatz should not be trusted far from the resonance region.

---

*Present address: TRIUMF, 4004 Wesbrook Mall, Vancouver, British Columbia, Canada V6T-2A3.

[1]Recent reviews or workshop summaries of the experimental and theoretical situation for the (p,π) reaction include, D. F. Measday and G. A. Miller, Annu. Rev. Nucl. Part. Sci. **29**, 121 (1979); B. Hoistad, Adv. Nucl. Phys. **11**, 135 (1979); H. W. Fearing, Prog. Part. Nucl. Phys. **7**, 113 (1981); in *Pion Production and Absorption in Nuclei—1981 (Indiana University Cyclotron Facility)*, Proceedings of the Conference on Pion Production and Absorption in Nuclei, AIP Conf. Proc. No. 79, edited by Robert D. Bent (AIP, New York, 1982); G. E. Walker, Comments Nucl. Part. Phys. **A11**, 169 (1983).

[2]D. B. Lichtenberg, Phys. Rev. **105**, 1084 (1957).

[3]M. Bertz *et al.*, in *Pion Production and Absorption in Nuclei—1981 (Indiana University Cyclotron Facility)*, Proceedings of the Conference on Pion Production and Absorption in Nuclei, AIP Conf. Proc. No. 79, edited by Robert D. Bent (AIP, New York, 1982), p. 65.

[4]F. Soga *et al.*, Phys. Rev. C **22**, 1348 (1980); F. Soga *et al.*, *ibid.* **24**, 570 (1981).

[5]A. Reitan, Nucl. Phys. **B29**, 525 (1971).

[6]Z. Grossman, F. Lenz, and M. P. Locher, Ann. Phys. (N.Y.) **84**, 348 (1974).

[7]M. Dillig and M. G. Huber, Phys. Lett. **69B**, 429 (1977).

[8]M. Hirata, Phys. Rev. Lett. **40**, 704 (1978).

[9]B. D. Keister and L. S. Kisslinger, Nucl. Phys. **A412**, 301 (1984).

[10]M. J. Iqbal, Ph.D. thesis, Indiana University, 1982 (unpublished) (copies available on request from G. E. Walker).

[11]A. de-Shalit and I. Talmi, *Nuclear Shell Theory* (Academic, New York, 1963), pp. 514—517.

[12]R. A. Freedman, G. A. Miller, and E. M. Henley, Nucl. Phys. **A389**, 457 (1982).

[13]The 200 MeV parameters are obtained from a best fit to 200 MeV $\vec{p}+{}^{12}C$ cross section and analyzing power data. The 250 MeV parameters are extrapolations of best fit parameters to 122—200 MeV $\vec{p}+{}^{12}C$ data. P. Schwandt (private communication).

[14]E. R. Siciliano and R. M. Thaler, Phys. Rev. Lett. **41**, 927 (1978).

[15]R. A. Eisenstein and G. A. Miller, Comput. Phys. Commun. **8**, 130 (1974).

[16]B. Holstad, S. Dahlgten, P. Grafstrom, and A. Asberg, Phys. Scr. **9**, 201 (1974).

[17]J. T. Londergan and G. D. Nixon, Phys. Rev. C **19**, 998 (1979).

[18]A. Arima, G. E. Brown, H. Hyuga, and M. Ichimura, Nucl. Phys. **A205**, 27 (1973).

[19]For 250 MeV data: G. J. Lolos *et al.*, TRIUMF Report No. TRI-PP-84-2, 1984; for 200 MeV data: F. Soga *et al.*, Phys. Rev. C **24**, 570 (1981).

[20]G. J. Lolos *et al.*, TRIUMF Report No. TRI-PP-84-2, 1984.